phases of glutamate release by different mechanisms. *Trends Neurosci.* **17,** 359–365 (1994).
10. Hansen, A. J. Effect of anoxia on ion distribution in the brain. *Physiol. Rev.* **65,** 101–148 (1985).
11. Basarsky, T. A., Feighan, D. & MacVicar, B. A. Glutamate release through volume-activated channels during spreading depression. *J. Neurosci.* **19,** 6439–6445 (1999).
12. Lerma, J. & Martin del Rio, R. Chloride transport blockers prevent N-methyl-D-aspartate receptor-channel complex activation. *Mol. Pharmacol.* **41,** 217–222 (1992).
13. Walz, W., Klimaszewski, A. & Paterson, I. A. Glial swelling in ischemia: a hypothesis. *Dev. Neurosci.* **15,** 216–225 (1993).
14. Sarantis, M. *et al.* Glutamate uptake from the synaptic cleft does not shape the decay of the non-NMDA component of the synaptic current. *Neuron* **11,** 541–549 (1993).
15. Spruston, N., Jonas, P. & Sakmann, B. Dendritic glutamate receptor channels in rat hippocampal CA3 and CA1 pyramidal neurons. *J. Physiol. (Lond.)* **482,** 325–352 (1995).
16. Madl, J. E. & Burgesser, K. Adenosine triphosphate depletion reverses sodium-dependent, neuronal uptake of glutamate in rat hippocampal slices. *J. Neurosci.* **13,** 4429–4444 (1993).
17. Storm-Mathiesen, J. *et al.* Ultrastructural immunocytochemical observations on the localization, metabolism and transport of glutamate in normal and ischemic brain tissue. *Prog. Brain Res.* **94,** 225–241 (1992).
18. Attwell, D., Barbour, B. & Szatkowski, M. Nonvesicular release of neurotransmitter. *Neuron* **11,** 401–407 (1993).
19. Levy, L. M., Warr, O. & Attwell, D. Stoichiometry of the glial glutamate transporter GLT-1 expressed inducibly in a CHO cell line selected for low endogenous Na^+-dependent glutamate uptake. *J. Neurosci.* **18,** 9620–9628 (1998).
20. Gundersen, V., Danbolt, N. C., Ottersen, O. P. & Storm-Mathisen, J. Demonstration of glutamate/aspartate uptake activity in nerve endings by use of antibodies recognizing exogenous D-aspartate. *Neuroscience* **57,** 97–111 (1993).
21. Zerangue, N. & Kavanaugh, M. P. Flux coupling in a neuronal glutamate transporter. *Nature* **383,** 634–637 (1996).
22. Billups, B. & Attwell, D. Modulation of non-vesicular glutamate release by pH. *Nature* **379,** 171–174 (1996).
23. Sah, P., Gibb, A. J. & Gage, P. W. Potassium current activated by depolarization of dissociated neurons from adult guinea pig hippocampus. *J. Gen. Physiol.* **92,** 263–278 (1988).
24. Nowicky, A. V. & Duchen, M. R. Changes in $[Ca^{2+}]_i$ and membrane currents during impaired mitochondrial metabolism in dissociated rat hippocampal neurons. *J. Physiol. (Lond.)* **507,** 131–145 (1998).
25. Jahr, C. E. & Stevens, C. F. Voltage dependence of NMDA-activated macroscopic conductances predicted by single-channel kinetics. *J. Neurosci.* **10,** 3178–3182 (1990).
26. Patneau, D. K. & Mayer, M. L. Structure-activity relationships for amino acid transmitter candidates acting at N-methyl-D-aspartate and quisqualate receptors. *J. Neurosci.* **10,** 2385–2399 (1990).
27. Raley, K. M. & Lipton, P. NMDA receptor activation accelerates ischemic energy depletion in the hippocampal slice and the demonstration of a threshold for ischemic damage to protein synthesis. *Neurosci. Lett.* **110,** 118–123 (1990).
28. Friedman, J. E. & Haddad, G. G. Anoxia induces an increase in intracellular sodium in rat central neurons in vitro. *Brain Res.* **663,** 329–334 (1994).
29. McBain, C. J., Traynelis, S. F. & Dingledine, R. Regional variation of extracellular space in the hippocampus. *Science* **249,** 674–677 (1990).
30. Roettger, V. & Lipton, P. Mechanism of glutamate release from rat hippocampal slices during in vitro ischemia. *Neuroscience* **75,** 677–685 (1996).

Acknowledgements

We thank E. Rutledge and H. Kimelberg for providing L-644,711, and J. Ashmore, P. Behe, S. Brickley, B. Clark, D. Colquhoun, F. Edwards, M. Farrant, A. Gibb, M. Hamann, M. Häusser and A. Silver for comments on the manuscript. This work was supported by the Wellcome Trust, European Community and the Shionogi Company Ltd.

Correspondence and requests for materials should be addressed to D.A. (e-mail: D.Attwell@ucl.ac.uk).

Blocker protection in the pore of a voltage-gated K^+ channel and its structural implications

Donato del Camino, Miguel Holmgren, Yi Liu & Gary Yellen

Department of Neurobiology, Harvard Medical School, 220 Longwood Avenue, Boston, Massachusetts 02115, USA

The structure of the bacterial potassium channel KcsA[1] has provided a framework for understanding the related voltage-gated potassium channels (Kv channels) that are used for signalling in neurons. Opening and closing of these Kv channels (gating) occurs at the intracellular entrance to the pore, and this is also the site at which many open channel blockers affect Kv channels[2–4]. To learn more about the sites of blocker binding and about the structure of the open Kv channel, we investigated here the ability of blockers to protect against chemical modification of cysteines introduced at sites in transmembrane segment S6, which contributes to the intracellular entrance. Within the intracellular half of S6 we found an abrupt cessation of protection for both large and small blockers that is inconsistent with the narrow 'inner pore' seen in the KcsA structure. These and other results are most readily explained by supposing that the structure of Kv channels differs from that of the non-voltage-gated bacterial channel by the introduction of a sharp bend in the inner (S6) helices. This bend would occur at a Pro-X-Pro sequence that is highly conserved in Kv channels, near the site of activation gating.

Figure 1 shows the results of a typical blocker protection measurement, for a cysteine introduced at position 474 in the S6

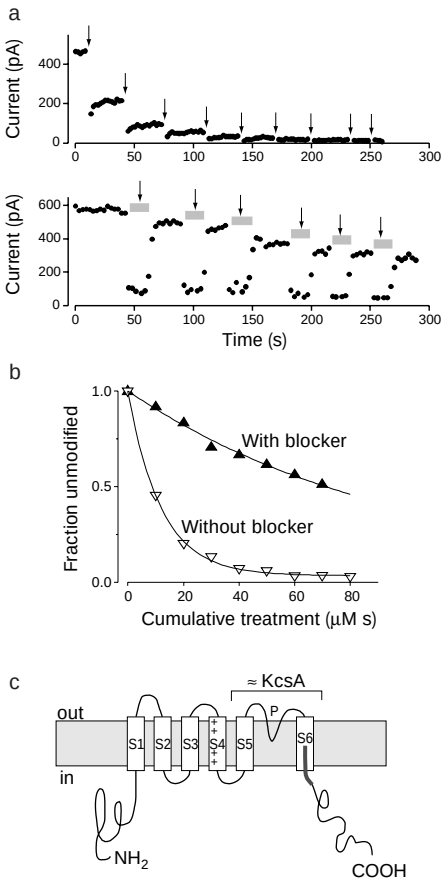

Figure 1 Tetrabutylammonium (TBuA) protects Cys 474 from MTSET modification. **a,** Chemical modification of 474C mutant channels. Top, the inside-out patch was held at −90 mV; dots indicate the steady-state current in response to brief pulses (20 ms) to +60 mV. At the times indicated by arrows, 20 μM MTSET was applied for 500 ms during a voltage step to +60 mV. Bottom, a similar experiment with modification performed in the presence of 60 μM TBuA. The channels were exposed to the blocker during the time showed by the horizontal bars; ~85% of the current was blocked. MTSET (40 μM) was applied for 250 ms in the open state as indicated by the arrows. **b**, Time course of the normalized current decrease as a result of modifications performed without or with 60 μM TBuA. The abscissa shows the cumulative reagent exposure (modification time × [MTSET]). The lines represent the best fit of the current reduction data to single exponential functions; the fit for the modification in the presence of blocker was constrained to use the final steady-state reduction seen in the control. The modification rate constant from the exponential fits was $\sim 8.3 \times 10^4\ M^{-1}s^{-1}$ without TBuA and $\sim 1.0 \times 10^4\ M^{-1}s^{-1}$ with blocker. Given the degree of blockade, this implies that blocked channels are almost completely unreactive (see Methods). **c**, Model of the membrane topology of a subunit of Shaker K^+ channel showing the region studied (thick line from positions 470 to 486). As indicated, the S5-P-S6 regions correspond to the sequence homology with the KcsA channel.

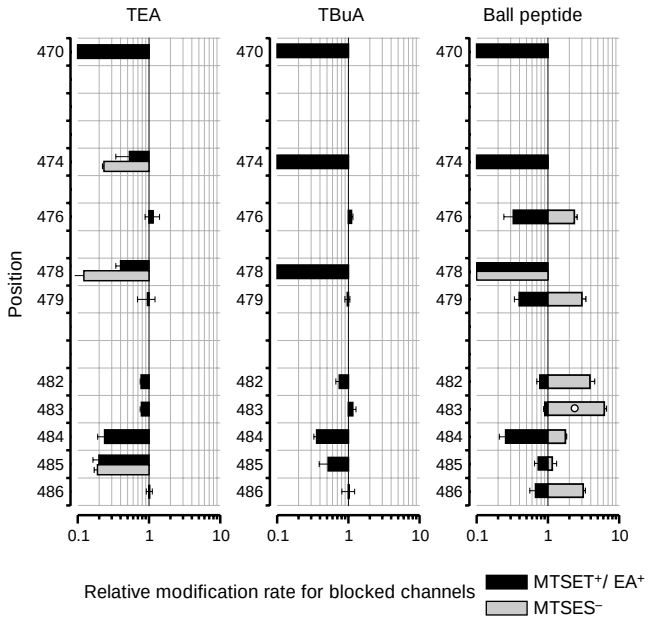

Figure 2 Effects of blocker on MTS reagent modification of cysteines introduced in S6. On a logarithmic axis, the bars represent the change in the modification rates produced by the blockers TEA, TBuA or ball peptide. Bars originate at 1 and end at a position corresponding to the relative modification rate for blocked channels (see Methods). Black bars, positively charged MTSET (or MTSEA, for 470C); grey bars, negatively charged MTSES. Modification at most positions was monitored by the reduction of current (see Methods). The open circle for ball peptide at position 483 shows the value of the relative modification rate for the uncharged reagent MTSACE. Bars that reach to 0.1 represent measured relative modification rates between zero and 0.1. For the modification rates for each residue measured in the absence of blocker, see Supplementary Information.

segment of a Shaker K^+ channel. The control modification rate was determined in an inside-out membrane patch containing many 474C channels (Fig. 1a, top) by repeated brief applications of MTSET (the linear methanethiosulphonate (MTS) derivative of ethyl(trimethylammonium)) to the intracellular surface. After each application there was a step reduction in the size of the current, and these steps were plotted to determine the modification rate constant (Fig. 1b). We performed a similar experiment in the presence of a blocker, tetrabutylammonium (TBuA; Fig. 1a, bottom). The two rate constants were compared (Fig. 1b), and the ratio was corrected for the fraction of channels that remained unblocked (see Methods). In this case, the relative modification rate for blocked channels was near zero.

We systematically applied this approach to determine the effects of three different open channel blockers—tetraethylammonium (TEA), tetrabutylammonium and the inactivation-related 20-amino-acid 'ball peptide'[5]—on modification of a series of S6 residues. The results are shown in Fig. 2 on a logarithmic scale: the bars to the left represent protection by bound blocker (a decrease in rate) and those to the right represent enhancement of modification by bound blocker.

We first consider results with the positively charged reagents MTSET and MTSEA (the MTS derivative of ethylamine; black bars). The clearest effects were the virtually complete protection (>10× reduction in modification rate) seen at three positions: 470, 474 and 478. These three positions were fully protected by the two larger blockers, TBuA and ball peptide. The result is consistent with the ideas that these three residues line the pore and that the blockers physically obstruct the pathway from the intracellular solution into the pore. The smaller blocker, TEA, produced complete protection only at the deepest of the three positions (470), indicating that it may penetrate more deeply into the pore. This conclusion is compatible with known differences between TEA and larger quaternary ammonium compounds in sensitivity to mutations[6] and in allosteric effects on C-type inactivation[7].

For many positions, the bound blockers had little or no effect on the cysteine modification rate. This was particularly striking in the case of position 476, which lies between two strongly protected residues (474 and 478) but was completely unaffected by the two blockers TEA and TBuA. This residue is thus likely to face away from the pore lining, in a position that allows access from the intracellular solution even when the pore is blocked. This result is consistent with the failure of Cd^{2+} binding or MTSET modification to prevent conduction through channels with a cysteine at this position, even though both treatments completely inhibit the 474C and 478C mutants[3].

There are many other effects and non-effects of blockers on modification whose interpretation is less obvious. To the extent that protection occurs by physical occlusion, weak or absent protection could result if the introduced cysteines are completely outside the pore and the binding site for the blockers. Alternatively, weak 'occlusive protection' could occur at a wide part of the pore where the blocker fails to cover simultaneously the cysteines in all four subunits. There are also two alternative mechanisms by which blockers may alter the modification rate: the positive charge on the blocker could repel the positively charged modifying agent (electrostatic), or the blocker could alter the structure of the protein to affect access to the site (allosteric).

The most testable of these is the electrostatic mechanism, which would predict a substantially greater effect for the ball peptide (with charge $q = +6$) than the other blockers (with $q = +1$). If a direct charge–charge interaction is responsible, we should be able to reverse the effect by using a negatively charged modification reagent, MTSES (the MTS derivative of ethylsulphonate). This reversal was seen for the effects of ball peptide at many positions: 476, 479, 482, 483, 484 and 486 (Fig. 2, grey bars). For two of these, 476 and 479, the effect of ball peptide on MTSES modification was equal and opposite to that on MTSET modification, and there was no effect of the two singly charged blockers; this is consistent with a purely electrostatic effect of the ball peptide on modification. At positions 476 and 486 we also found a strong reciprocal effect on ball peptide affinity when the cysteines were modified with charged reagents. Modification with MTSET substantially reduced ball peptide affinity, whereas modification with MTSES increased its affinity (data not shown). These results argue that the electrostatic effect involves a direct interaction between the modified cysteines and the charged ball peptide. Thus the ball peptide must bind physically near these sites, as previously shown for a site in the S4–S5 linker[8].

The other sites of electrostatic interaction showed asymmetrical effects, which probably represent a combination of electrostatic and other (allosteric or weak occlusive) effects. We tested this idea at position 483 using an uncharged modification reagent, MTSACE (the MTS derivative of propionamide). The effect of ball peptide on modification with this reagent was intermediate between its effects on MTSET and MTSES, and probably represents an allosteric effect on modification at this site. Other, unexplained allosteric effects occurred at position 484 for all three blockers and at position 485 (where the effect was strongest for TEA). (Although the state dependence of cysteine modification[3] at these two positions is weak by comparison with the deeper part of the pore, there are 3- to 6-fold changes in accessibility that are compatible with some movement. The known effects of the blockers on gating state do not, however, explain the allosteric protection.)

How do the protection results fit with the known structure of another K^+ channel, KcsA, which is not voltage-gated? The failure of the ball peptide to produce any strong protection below the level of position 478 is unexpected. This result on open Kv channels is apparently inconsistent with the KcsA crystal structure. In KcsA there is a narrow 'inner pore' below the level of the bundle crossing

formed by the inner helices (Fig. 3). If the ball peptide blocked the inner pore at the intracellular entrance, any side chain facing the inner pore would be protected strongly by the blockade: we would thus expect at least one of the residues in the range 482–486 to be strongly protected. The contradiction is most apparent when the pore surface of KcsA is coloured with the protection results from Shaker, and the blockers are viewed on the same scale as the KcsA structure (Fig. 3).

Flexibility or loose packing of the inner pore lining might explain why it remains accessible to reagent even when ball peptide is bound, but it would then become harder to explain why potassium ion flow is blocked by the ball. It is possible that the peptide binding produces a remote (allosteric) action that closes the pore to potassium ions at a higher level (around 478), but there is evidence that the ball acts by physically occluding the pore[5,9,10]. In particular, TEA and the ball peptide act competitively[9], an observation most simply consistent with pore blockade. The kinetics of ball peptide action[5] and the ability of elevated extracellular [K^+] to speed recovery from inactivation[10] also support the idea that the ball peptide acts by directly occluding the pore.

An alternative model to explain the protection results is that in the Kv channels the S6 helix is bent near the intracellular surface of the membrane (Fig. 4), unlike the linear inner helices of KcsA. This would be a natural consequence of the sequence Pro-X-Pro at positions 473–475, which is absolutely conserved among all Kv channels but is not found in KcsA or in Kir channels. In known protein structures, single prolines generally introduce a kink of about 26° in a helix, because they eliminate a backbone hydrogen bond[11]. The sequence PxP, which would break two hydrogen bonds within one helical turn, almost never occurs within a helix except within the first turn[11] (see Methods). In general, the PxP sequence produces a complete disruption of helical structure, with two helices separated by a break of about four or more nonhelical residues that permit a turn of almost any angle. Of course, initial attempts at modelling the Kv channel structure predicted a bend in S6 at the PxP sequence[12] (the lower S6 was proposed to remain roughly perpendicular to the membrane). But since the publication of the KcsA structure[1] and its good agreement with the functional work on Shaker[3,4,13], it has been widely assumed that the KcsA linear inner helices were a good model for the Kv channel S6 structure.

The 'bent S6' model of Fig. 4 fits well with the protection results because below the point of the bend (assumed to span roughly from 473 to 476) the pore would become quite broad. The ball peptide could then bind to this broad face, covering the entrance but not aligned with the centre (analogous to the binding of agitoxin to the extracellular entrance of Shaker channels[14]). There would be few positions that exhibit strong protection—because the ball peptide would not cover all four subunits at once—but many positions that could interact with the peptide electrostatically.

In a mutant Shaker channel with a cysteine at position 476, Cd^{2+} ions can lock the channel open by forming an intersubunit bridge between this cysteine and the histidine at position 486 in the neighbouring subunit[13]. Qualitatively this result fit well with the 'bundle crossing' seen in the KcsA structure: the intersubunit bridge would stabilize the bundle in the open configuration, whereas during normal closing the bundle would rearrange and pinch the channel shut at its narrowest point[3,4]. Quantitatively, though, these positions are located too far apart in the KcsA structure for a bridge to form: based on the position of the KcsA backbone, the S_γ–N_ϵ distance would be at least 13Å (Fig. 4, left), compared with a distance in zinc finger proteins of ~ 3.6Å (see, for example, ref. 15). The 'bent S6' model of Fig. 4 would also resolve this problem, allowing the bridge to form between neighbouring subunits (the hypothetical positions of the Cys-Cd^{2+}-His bridges are shown in the Figure). Moreover, it allows direct access from the intracellular

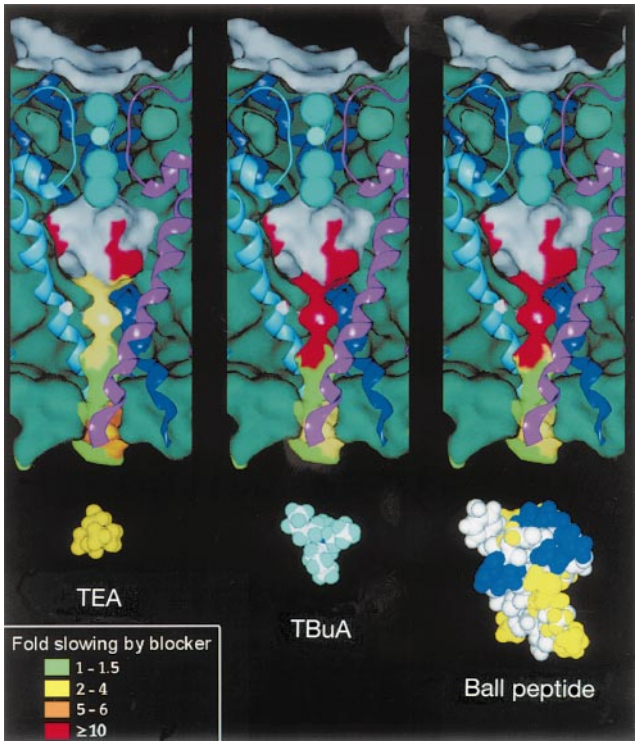

Figure 3 Protection results for three blockers overlaid on the lining of the KcsA pore. Each view shows the KcsA skeleton, with the inner helices crossing near the bottom (one of the four subunits has been removed to permit viewing). The selectivity filter loop is at the top, with three K^+-binding positions (large cyan balls) and one water molecule (small cyan ball) indicated. The protein surface is a grey shell (dark green from the interior), and the surfaces of the central cavity and inner pore are coloured using the MTSET and MTSEA protection results from Fig. 2. Below the protection pattern for each blocker is a space-filling structure of the blocker. In the case of ball peptide, the first 20 residues of one of the nuclear magnetic resonance structures for the Kv3.4 ball[27] are shown, with the basic residues coloured dark blue. The blockers are shown for approximate size and not for exact structure, which is probably mobile. However, even if the bound ball peptide were to adopt a completely different structure, there is too much mass for it to fail to protect the lower S6 if it acts by plugging a pore with the approximate structure of KcsA. The Figure was generated using the program SPOCK (J. Christopher, Texas A & M University).

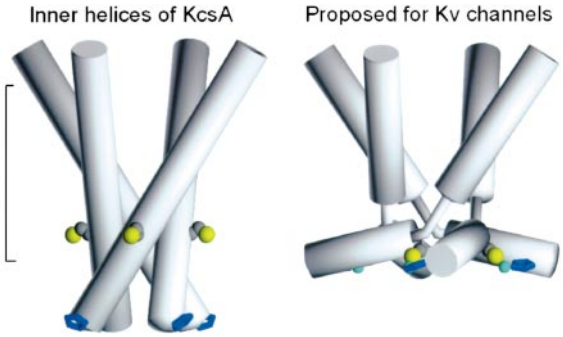

Figure 4 The 'bent S6' model for Kv channels compared with the inner helices of KcsA. The positions of the KcsA inner helices are approximated by four cylinders, one from each subunit. The square bracket next to KcsA shows the approximate extent of the membrane, as judged from the positions of tryptophan layers in the KcsA structure. For Kv channels, the S6 segments are shown as two helices with an intervening bend, proposed to occur near the two prolines at positions 473 and 475. The intracellular entrance is at the bottom, and the bend produces a broad vestibule just below the bundle crossing. The hypothetical position of the intersubunit bridges Cys476-Cd^{2+}-His486 are shown for the Kv channels (yellow ball, cysteine sulphur; cyan sphere, Cd^{2+}; blue pentagon, histidine imidazole ring). For comparison, cysteine and histidine have been shown at the analogous position in KcsA. This Figure was derived from the KcsA structure[1] and from an exploratory molecular model of the Kv structure (prepared with Insight 98.0 (Molecular Simulations) and exported to a drawing program).

surface to the cysteine at 476; previously it was necessary to suppose that there was a crevice on the back side of the pore-lining helices to permit such access.

This 'bent S6' model for voltage-gated K^+ channels is as faithful as possible to the one known structure of a related protein, KcsA. The addition of a bend is based on the behaviour in known protein structures of the Pro-X-Pro sequence, which is conserved absolutely among voltage-gated K^+ channels and is not found in KcsA. The change is mandated by the qualitative constraint on the Kv pore structure imposed by the protection results—the pore becomes broad below the bundle crossing—and by the quantitative distance constraint imposed by the 476C-Cd^{2+}-H486 intersubunit bridge. The resulting picture provides an improved basis for further functional work on Kv channels.

The protection data and the Cd^{2+} bridge pertain only to the open state of Kv channels, so it is possible that the Kv channels adopt a KcsA-like structure when they close. Indeed, for KcsA there is evidence that pH-induced gating involves a separation of the lower part of the inner helices[16]. Because the spin-labelling data do not permit a quantitative estimate of the changes in distance, it cannot be ruled out that the inner helices may splay out as we propose for the Kv channels, rather than moving as a rigid body as proposed in ref. 16. However, the idea that the Kv channels close to a KcsA-like structure with a narrow inner pore does not seem compatible with the small state-dependent accessibility seen for the lower S6 helix[3], even for reagents larger than MTSET (D.D.C. and G.Y., unpublished data). We therefore suspect that the Kv channels have a bent S6 in both the open and closed states. Because the bend occurs quite near the site at which activation gating closes the pore[3], it seems possible that gating involves a structural change at the bend. □

Methods

Mutagenesis and expression

We introduced mutations into a Shaker H4 potassium channel[17] containing three additional modifications: a deletion between residues 6 and 26 that removes N-type inactivation[18], substitution of cysteines 301 and 308 by serines to diminish the wild-type effect of chemical modification[8], and mutation of threonine 449 to valine to reduce C-type inactivation[19]. Channels were transiently expressed in human embryonic kidney (HEK)293 cells and used 1–3 days after transfection. Methods for mutagenesis, transfection and identification of transfected cells have been described[20]. The tandem dimers were subcloned into a construct prepared by L. Heginbotham and R. MacKinnon[21].

Physiological recording

All experiments were performed on inside-out excised patches[22]. Standard experimental solutions contained, in mM: 60 NaCl, 100 KCl, 3 $CaCl_2$, 1 $MgCl_2$ and 10 HEPES, at pH 7.4 (pipette); and 160 KCl, 0.5 $MgCl_2$, 1 EGTA and 10 HEPES, at pH 7.4 (bath). Solutions with Cd^{2+} contained no EGTA. The methods for electrophysiological recordings and rapid perfusion switches have been described[3,8].

Synthetic ball peptides

Unless stated otherwise, 'ball peptide' experiments were performed with the E12K, D13K ball peptide[23], which is a double mutant of the 20-amino-acid Shaker inactivation peptide[5] with increased positive charge (two positively charged residues replace two negatively charged residues). In several cases, we compared the effects of the wild-type Shaker ball peptide. Both ball peptides were synthesized, purified by HPLC and then amidated at the carboxy terminus by the Massachusetts General Hospital peptide synthesis facilities.

Chemical modification and analysis of blocker effects

MTS reagents were purchased from Toronto Research Chemicals Inc. These reagents were prepared as stocks in water each day, held on ice and mixed into the recording solution immediately before use. At most positions, we used the reduction in current to monitor modification, but when this change was small or absent we used other methods. At position 476 we measured the fraction of current with altered gating. The loss of Cd^{2+} sensitivity was used at positions 483 and 486 for MTSET, and also at position 484 for MTSES. Current increase was measured at positions 482, 483 and 486 for MTSES. Positions 471, 472, 473 and 480 were not substantially affected by MTSET or MTSEA treatment. 479C mutant channels were studied as tandem dimers, with only one of the two protomers containing the mutation (this mutant did not express functionally as homotetramers); the F481C mutant did not express even as a tandem dimer. The cysteine mutants at position 475 (normally prolines) were not included in this study because the mutant itself has pronounced effects on gating and blockade. The cysteine at position 477 has a much lower reaction rate than its neighbours and was also not included. MTSEA was the only reagent that produced a measurable effect on 470C. We obtained the reaction rates by measuring the time course of the effect caused by the modification upon repeated brief application of the MTS reagent under conditions of maximum open probability. We calculated modification rate constants by taking the reciprocal of the time constant of a monoexponential fit to the time course of modification and dividing by [MTS] (Fig. 1; also ref. 3). The effect of the blockers was assessed by measuring the modification rate constant in the presence or absence of the blocker, using control experiments done with the same MTS stock solution on the same day. For the channel blockers used here, it has been established kinetically that a single molecule of blocker produces the blockade, so we can consider that in the presence of the blocker, channels are in two states: unblocked or blocked[5,24,25]. In a non-saturating concentration of blocker we measured the fraction unblocked (f_{UB}) directly from the ratio of the current in the presence of blocker to the current in its absence. The measured rate constant for modification in the presence of blocker ($k_{overall}$) is then $k_{overall} = f_{UB} \cdot k + (1-f_{UB}) \cdot k'$, where k and k' are the modification rate constants for unblocked and blocked channels, respectively. The rate constant k was measured directly, and k' was computed from the measurements of k, $k_{overall}$ and f_{UB}. The ratio $r \equiv k'/k$ gives the relative modification rate for the blocked channels (plotted in Fig. 2 for many positions and several reagents). Small values of r correspond to strong protection; $r = 1$ corresponds to no protection; and $r > 1$ means that the blocked channels react faster than the unblocked channels.

Analysis of Pro-X-Pro in the protein data bank

To allow us to check the conclusions of ref. 11 on newer structures, the authors (M. W. MacArthur and J. M. Thornton) performed a search[26] for non-redundant structures containing the PxP motif with at least one α-helical residue in the ten residues preceding and one in the nine residues following the first proline, to identify prolines in an α-helical context. Of the ~100 structures selected in this way, almost all have four or more non-helical residues between two helical segments. The 14 structures with the highest assigned helical content around the PxP were examined and found to have breaks between the two helices, with an interhelix angle between ~35° and 180° (a hairpin). One structure, represented by entry 1PHB (cytochrome P450), had a short helix preceding PxP that was bent only ~20° relative to the helix following.

Received 17 August; accepted 6 December 1999.

1. Doyle, D. A. *et al.* The structure of the potassium channel: molecular basis of potassium conduction and selectivity. *Science* **280,** 69–77 (1998).
2. Armstrong, C. M. Interaction of tetraethylammonium ion derivatives with the potassium channels of giant axon. *J. Gen. Physiol.* **58,** 413–437 (1971).
3. Liu, Y., Holmgren, M., Jurman, M. E. & Yellen, G. Gated access to the pore of a voltage-dependent K^+ channel. *Neuron* **19,** 175–184 (1997).
4. Yellen, G. The moving parts of voltage-gated ion channels. *Q. Rev. Biophys.* **31,** 239–296 (1998).
5. Zagotta, W. N., Hoshi, T. & Aldrich, R. W. Restoration of inactivation in mutants of Shaker K^+ channels by a peptide derived from ShB. *Science* **250,** 568–571 (1990).
6. Choi, K. L., Mossman, C., Aubé, J. & Yellen, G. The internal quaternary ammonium receptor site of Shaker potassium channels. *Neuron* **10,** 533–541 (1993).
7. Baukrowitz, T. & Yellen, G. Two functionally distinct subsites for the binding of internal blockers to the pore of voltage-activated K^+ channels. *Proc. Natl Acad. Sci. USA* **93,** 13357–13361 (1996).
8. Holmgren, M., Jurman, M. E. & Yellen, G. Structure and function of the S4–S5 loop of the *Shaker* K^+ channel examined through cysteine mutagenesis and chemical modification. *J. Gen. Physiol.* **108,** 195–206 (1996).
9. Choi, K. L., Aldrich, R. W. & Yellen, G. Tetraethylammonium blockade distinguishes two inactivation mechanisms in voltage-activated K^+ channels. *Proc. Natl Acad. Sci. USA* **88,** 5092–5095 (1991).
10. Demo, S. D. & Yellen, G. The inactivation gate of the Shaker K^+ channel behaves like an open-channel blocker. *Neuron* **7,** 743–753 (1991).
11. MacArthur, M. W. & Thornton, J. M. Influence of proline residues on protein conformation. *J. Mol. Biol.* **218,** 397–412 (1991).
12. Durell, S. R. & Guy, H. R. Atomic scale structure and functional models of voltage-gated potassium channels. *Biophys. J.* **62,** 238–247 (1992).
13. Holmgren, M., Shin, K. S. & Yellen, G. The activation gate of a voltage-gated K^+ channel can be trapped in the open state by an intersubunit metal bridge. *Neuron* **21,** 617–621 (1998).
14. Gross, A. & MacKinnon, R. Agitoxin footprinting the Shaker potassium channel pore. *Neuron* **16,** 399–406 (1996).
15. Lee, M. S., Gippert, G. P., Soman, K. V., Case, D. A. & Wright, P. E. Three-dimensional solution structure of a single zinc finger DNA-binding domain. *Science* **245,** 635–637 (1989).
16. Perozo, E., Cortes, D. M., & Cuello, L. G. Structural rearrangements underlying K^+ -channel activation gating. *Science* **285,** 73–78 (1999).
17. Kamb, A., Tseng-Crank, J. C. L. & Tanouye, M. A. Multiple products of the *Drosophila* Shaker gene may contribute to potassium channel diversity. *Neuron* **1,** 421–430 (1988).
18. Hoshi, T., Zagotta, W. N. & Aldrich, R. W. Biophysical and molecular mechanisms of Shaker potassium channel inactivation . *Science* **250,** 533–538 (1990).
19. López-Barneo, J., Hoshi, T., Heinemann, S. H. & Aldrich, R. W. Effects of external cations and mutations in the pore region on C-type inactivation of Shaker potassium channels. *Receptors Channels* **1,** 61–71 (1993).
20. Jurman, M. E., Boland, L. M., Liu, Y. & Yellen, G. Visual identification of individual transfected cells for electrophysiology using antibody-coated beads. *BioTechniques* **17,** 876–881 (1994).
21. Heginbotham, L. & MacKinnon, R. The aromatic binding site for tetraethylammonium ion on potassium channels. *Neuron* **8,** 483–491 (1992).
22. Hamill, O. P., Marty, A., Neher, E., Sakmann, B. & Sigworth, F. J. Improved patch-clamp techniques for high-resolution current recording from cells and cell-free membrane patches. *Pflügers Arch.* **391,** 85–100 (1981).
23. Murrell-Lagnado, R. D. & Aldrich, R. W. Interactions of amino terminal domains of Shaker K channels with a pore blocking site studied with synthetic peptides. *J. Gen. Physiol.* **102,** 949–975 (1993).
24. Armstrong, C. M. Time course of TEA^+-induced anomalous rectification in squid giant axons. *J. Gen.*

Physiol. **50,** 491–503 (1966).
25. Swenson, R. P. Jr Inactivation of potassium current in squid axon by a variety of quaternary ammonium ions. *J. Gen. Physiol.* **77,** 255–271 (1981).
26. Gardner, S. & Thornton, J. Iditis: protein structure database. *Acta Crystallogr. D Biol. Crystallogr.* **54,** 1071–1077 (1998).
27. Antz, C. *et al.* NMR structure of inactivation gates from mammalian voltage-dependent potassium channels. *Nature* **385,** 272–275 (1997).

Supplementary Information is available from *Nature*'s World-Wide Web site (http://www.nature.com) or as paper copy from the London editorial office of *Nature*.

Acknowledgements

We thank Ki Soon Shin for performing some preliminary experiments with MTSES; M. MacArthur and J. Thornton for performing a database search; T. Ogren for help with the cells; B. Bean for comments on the manuscript; and members of the Yellen laboratory for helpful discussions. The work was supported by an NIH (NINDS) grant to G.Y., a fellowship from the Muscular Dystrophy Association to M.H. and a fellowship from the Spanish Ministry of Education to D.D.C.

Correspondence and requests for materials should be addressed to G.Y. (e-mail: gary_yellen@hms.harvard.edu).

KIR expression on self-reactive CD8$^+$ T cells is controlled by T-cell receptor engagement

Bertrand Huard*†‡ **& Lars Karlsson***

* *The R.W. Johnson Pharmaceutical Research Institute, 3210 Merryfield Row, San Diego, California 92121, USA*
† *Laboratoire d'immunologie des tumeurs, Tour E2, 1er étage, Faculté de Pharmacie de Chatenay-Malabry, 5 rue Jean Baptiste Clément, 92296 Chatenay-Malabry, France*

Natural killer cell tolerance is maintained by the interaction of killer inhibitory receptors (KIRs) with self-major histocompatibility complex class I gene products. A subset of T cells also expresses inhibitory receptors, but the functional significance of these receptors on T cells is unclear[1–3]. Here we show that, in the absence of T-cell receptor (TCR) engagement, KIRs expressed on CD8$^+$ T cells are slowly downregulated by KIR ligands expressed on antigen-presenting cells. The resulting expression levels of KIR are no longer able to inhibit T-cell function. In contrast, TCR engagement sustains KIR expression, and re-induces functional levels of KIR expression after ligand-induced downregulation of KIR. Our data indicate that KIR expression on CD8$^+$ T cells *in vivo* may be maintained through continuous encounters with antigen. As KIR-mediated inhibition of T-cell activation can be bypassed at high antigen concentrations, dynamic KIR expression may mediate T-cell tolerance to self-antigens by sparing self-reactive T cells, thus enabling them to mediate potentially useful immune functions to quantitatively or qualitatively different antigens.

Human NK and T cells express two families of MHC class I reactive inhibitory receptors: immunoglobulin-like receptors (for example, KIR) directly interact with various MHC class I molecules (human leukocyte antigen (HLA)-A,-B,-C and -G)[4–6]; and lectin-like receptors (CD94/NKG2), which interact with HLA-E-presenting signal-sequence peptides derived from other MHC class I molecules[7–9].

Although expression of CD94/NKG2 can be induced on T cells by certain cytokines[10], expression of KIRs on natural killer (NK) and T cells is believed to be stable over time and independent of cellular activation[10,11]. We observed that incubation of the KIR2D-expressing CD8$^+$ T-cell clone 1.15 (which is specific for an HLA-A2.1-restricted peptide derived from the melanocyte antigen tyrosinase[12]) with .221-A2.1-Cw7 cells (generated by transfection of the HLA-A, -B and -C-deficient cell line 721.221 (ref. 13) with HLA-A2.1 and HLA-Cw7 (a KIR2D ligand)) resulted in down-regulation of KIR2D from the T-cell surface when antigenic peptide was absent (Fig. 1a). After 24 hours, the KIR2D expression was reduced to 18% of the

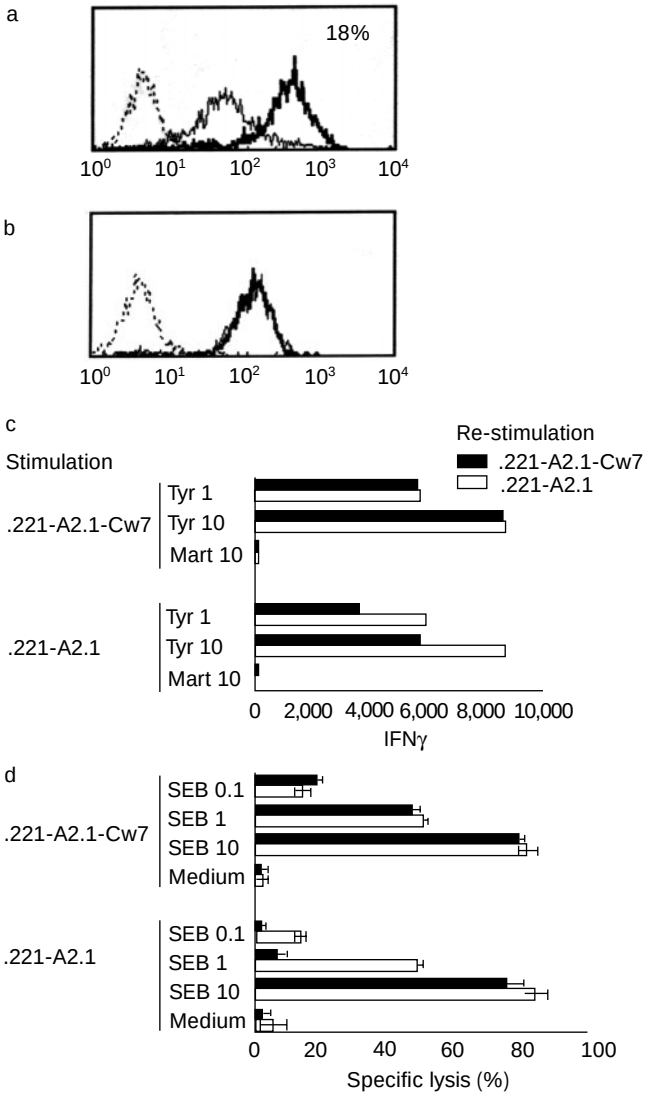

Figure 1 HLA ligands on APCs reduce KIR expression on T cells to non-functional levels. KIR2DL-expressing CD8$^+$ T-cell clone 1.15 (**a**) or a KIR2DS-expressing CD8$^+$ T-cell clone (**b**), both specific for a tyrosinase peptide presented by HLA-A2.1, were incubated with irradiated .221-A2.1 or .221-A2.1-Cw7 cells in the presence of an irrelevant peptide (mart-1). After 48 hours, KIR2DL expression was reduced to 18%, as assessed by immunofluorescence staining and flow cytometry analysis on gated T cells (BMA-031 staining). Thick and thin lines correspond to T cells incubated with .221-A2.1 and .221-A2.1-Cw7 cells, respectively. Dashed line represents background staining obtained with a control monoclonal antibody. **c**, KIR2D function after downregulation was assessed in a short-term re-stimulation assay. T-cell clone 1.15, previously incubated with the indicated APCs for 48 hours, was re-stimulated with .221-A2.1 (open bars) or with .221-A2.1-Cw7 (filled bars) cells loaded with peptides as indicated. Tyr, tyrosinase; Mart = mart-1, at 1 or 10 μM). Intracytoplasmic IFNγ was stained, analysed by flow cytometry on gated T cells and quantified (arbitrary units). A representative experiment is shown. **d**, A SEB reactive KIR2D-expressing T-cell clone, B16, was incubated with .221-A2.1 or .221-A2.1-Cw7 cells as in **a**. After 48 hours, the cytotoxic activity of T cells against .221-A2.1 (open bars) or .221-A2.1-Cw7 (filled bars) cells pulsed with medium alone or pulsed with SEB (μg ml^{-1}) was assessed in a ^{51}Cr-release assay. Error bars, ±s.d.

‡ Present address: Dermatology laboratory 5.222, Centre Médical Universitaire, 1 rue Michel Servet, CH-1211 Genève 4, Switzerland.